

THE PHYSICS OF THE HII REGIONS: THE PHOTOIONIZATION EQUILIBRIUM IN THE HII REGIONS OF M51

LEONEL GUTIÉRREZ^{1,2}, JOHN E. BECKMAN^{1,3}

1 Instituto de Astrofísica de Canarias. C/Vía Láctea s/n, La Laguna, 38200, Tenerife (SPAIN)

2 Universidad Nacional Autónoma de México, Apartado Postal 877, Ensenada 22800, Baja California (México)

3 Consejo Superior de Investigaciones Científicas (Spain)

Abstract: A general overview of the physical properties of the HII regions is presented here, emphasizing the various general models made to explain their structure and behaviour. The Lyman continuum effective extinction, representing a measure of the extinguished or lost fraction of the ionizing flux, is explained briefly, and the results of a study performed on this matter are presented. This study, based on a sample of about 200 HII regions of the galaxy M51 using high resolution images acquired with the HST, suggests a highly inhomogeneous structure.

Keywords: HII regions – Star formation rate – Extinction.

1 Introduction

A simple measure of the star formation rate (SFR) in a galaxy is the H α luminosity emitted by the ionized gas in the galaxy. However, according to the evidence, the H α luminosity is not completely satisfactory as a star formation indicator. Several factors, notably the extinction produced by the dust both of the H α luminosity and of the Lyman continuum before it can ionize the gas, do not permit an exact measurement of the SFR using only the H α luminosity. For highly obscured star-forming regions, a better tracer of SFR could be the total infrared emission (IR) [1], mainly the mid-IR. This has been confirmed by several studies carried out using data at 7 and 15 μm [2], at 6.7, 12, and 15 μm [3] and 24 μm [4, 5, 6, 7]. The results of Relaño et al. [7] show that the 24 μm luminosity can be used as a SFR tracer in individual HII regions, but for the integrated emission from entire galaxies it is necessary to take into account the metallicity of the galaxy. In addition, Calzetti et al. [8] found that the 8 μm emission shows strong dependence on metallicity and on the size of the region being

measured; also, they found that the $24\ \mu\text{m}$ emission bears a nonlinear relation with the $\text{Pa}\alpha$ emission (another useful tracer of SFR, but ~ 8 times weaker than $\text{H}\alpha$). On the other hand, even assuming that an important fraction of the luminous energy emitted by recently formed stars is reprocessed by dust in the infrared, there is a possible problem: the evolved stellar population also heats the dust giving an overestimate of the SFR. So, the best SFR tracer may well be a combination of $24\ \mu\text{m}$ and $\text{H}\alpha$ emission. However, in any case it is important to understand the efficiency of the ionization process in HII regions and know the behaviour of the dust in a galaxy in order to estimate its effects on the determination of the SFR.

M51 is a spiral galaxy (NGC 5194) interacting with its companion NGC 5195. Its essentially face-on orientation ($i \sim 40$ degrees) allows us to observe its structure with excellent detail and with a minimum of obscuration by interstellar dust. This makes it one of the best extragalactic systems for studying star formation.

The statistical properties as well as the physical properties of the HII regions of M51 have been studied by various authors, from Carranza et al. [9], to Calzetti et al. [5]. However, the aim of the present work is, using high resolution images, to quantify the missing fraction of Lyman continuum photons that are extinguished before ionizing the gas or simply escape from the region. These results can give us evidence about whether the gas and dust distribution are homogeneous.

To do that, a set of HII regions (about 200), with distances from the galaxy centre of between 5 and 11 kpc, has been analysed identifying by their colours the star clusters which are responsible for the gas ionization there. The Lyman continuum luminosity which should be produced by the clusters was calculated, as well as the $\text{H}\alpha$ luminosity which would be emitted if the gas were ionized in ideal conditions. Comparing this luminosity with the measured value corrected for extinction, we found values for the Lyman continuum effective extinction that reinforce the idea that the gas and dust distribution are very inhomogeneous.

2 The HII regions and models of their structure

When big clouds of interstellar gas collapse, they give rise to the formation of stars and star clusters. Once the stars are formed in the interior of a giant molecular cloud, many of them, the younger and more massive stars ($M_* > 10 M_\odot$) with high surface temperatures ($3 \times 10^4 \text{K} < T < 5 \times 10^4 \text{K}$), are stars of spectral type O and B which are generally grouped in “OB associations”. They are intense sources of UV radiation and release significant fluxes of photons with energies greater than 13.6 eV (the ionization potential of hydrogen) ionizing the surrounding hydrogen. This ionized gas becomes an HII region, usually surrounded by the neutral hydrogen shielded from the UV radiation. The higher the temperature and luminosity of the ionizing stars, the more luminous is the UV radiation and the higher is the ionization degree of the region [10,

11].

Hydrogen is the main constituent of the interstellar gas, hence it is the main component of the HII regions. However, it is possible to find in these regions other heavier elements in ionized states, mainly He, O, N, C and Ne simply or multiply ionized.

The electrons (or, better, photoelectrons) released in the ionization process, with local densities in the range $10 - 10^4 \text{ cm}^{-3}$, have kinetic energies given by the difference between the energy of the ionizing photon and the ionization potential of hydrogen. These electrons collide with other electrons and ions distributing their kinetic energy maintaining a maxwellian velocity distribution which defines the electron temperature of the HII region. Typically, this temperature is of order 7000 – 13000 K.

The electron-ion collisions can excite atoms of other types in the region, which emit in forbidden spectral lines. Among the more representative ions, excited in this way, are O^+ , O^{++} , N^+ , S^+ , S^{++} , emitting in the lines [OII], [OIII], [NII], [SII] and [SIII], respectively. Moreover, the recombination of these “thermalized” electrons with the excited ions (generally H^+ and He^+), followed by downward transitions in the energy level, give rise to the emission of “recombination lines” which, with the forbidden lines, dominate the emission spectrum of an HII region.

Hydrogen is globally ionized in an HII region and accounts for more than 75% of the mass of the region. So we can consider the ionization structure of the hydrogen as a first approximation to the global structure of the region. Therefore, let us idealize the region as a sphere with uniform density and volume $\frac{4}{3}\pi R_s^3$, in which, in a unit time, the number of ionizing photons (Q_o) emitted by the stars lying inside is equal to the number of electron-ion recombinations. The flux falls with the distance to the ionizing stars due to geometric dilution and absorption along the path of the photons, until it reaches a level where the ionization and recombination rates are in equilibrium. This radius R_s corresponds to this “borderline” and it is named the *Strömgren Radius* [10]. To compute this radius, we can assume that the region is optically thick and that the “on-the-spot” assumption is valid [11], i.e. there exists a high probability for the ionizing photons to be absorbed so that the recombinations to the ground state release photons immediately absorbed by other atoms nearby, with no net effects on the global ionization of the region (this is the so called “case B”). So, if N_p and N_e are the ion and electron densities, respectively, assumed constant inside the region, the total number of recombinations to excited levels will be given by $\frac{4}{3}\pi R_s^3 N_p N_e \alpha_B$, where α_B is the recombination coefficient to all the excited levels of the hydrogen.

Because we assume that the hydrogen is fully ionized, then $N_e = N_p \sim N_H$ and

$$Q_o = \frac{4}{3}\pi R_s^3 N_H^2 \alpha_B \quad (1)$$

Spectral type	T(K)	log(Q_o) (photons/sec)	R_s (pc)	
			$N_H \sim 1cm^{-3}$	$N_H \sim 10cm^{-3}$
O5	40900	49.22	80	17
O6	38900	48.99	67	14
O7	36900	48.75	56	12
O8	34900	48.44	44	9
O9	32900	48.06	33	7
O9.5	31900	47.88	29	6

Table 1: Strömgren radius R_s as a function of the spectral type of the star and of the density of the surrounding hydrogen.

where N_H is the hydrogen density in atoms cm^{-3} . Then, the Strömgren radius is given by

$$R_s = \left(\frac{3Q_o}{4\pi N_H^2 \alpha_B} \right)^{\frac{1}{3}} \quad (2)$$

The radius R_s defines a geometrically well defined transition from a sphere of fully ionized hydrogen to the neutral hydrogen surrounding it. Several values for R_s are shown in Table 1 assuming that the ionizing source is an individual star and considering the values for Q_o given by Martins et al. [12]. The thickness of the transition zone is approximately equal to one mean free path of an ionizing photon, i.e. $d \sim \frac{1}{a(\nu)N_H}$, where $a(\nu)$ is the ionization cross section for H by photons with energy $h\nu$, which must be higher than the 13.6 eV threshold. Typically $a(\nu) \sim 6 \times 10^{-18} cm^2$. So, with $N_H \sim 1 cm^{-3}$, the thickness is $d \sim 0.05 pc$, and with $N_H \sim 10 cm^{-3}$, $d \sim 0.005 pc$, small compared with the typical sizes of the HII regions (see Table 1).

The degree of ionization of the other chemical elements in the region depends on the distance to the ionizing star and on the effective stellar temperature. The second most abundant element after hydrogen is helium. In this case, the first ionization potential is 24.6 eV and the second one is 54.4 eV, so that only a very small quantity of doubly ionized He exists in HII regions because even the hottest O stars emit few photons more energetic than 54.4 eV. Photons with energy in the range 13.6 – 24.6 eV ionize the hydrogen and those with energy greater than 24.6 eV can ionize the helium too. Depending on the ionizing star temperature, also ions of other less abundant elements such as O^{++} , N^{++} and Ne^{++} may be found.

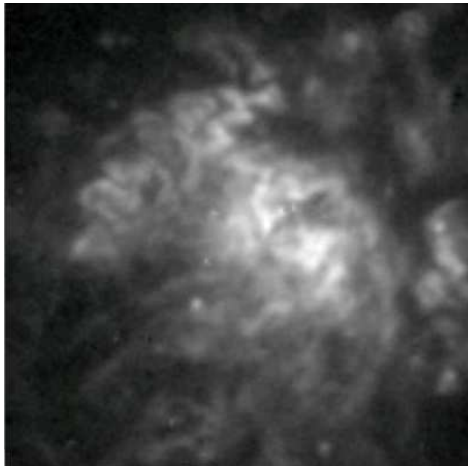


Figure 1: One of the HII regions of M51 showing its complex structure. This image spans over $7.5'' \times 7.5''$ ($\sim 300pc \times 300pc$).

2.1 Ionization bounded and density bounded HII regions

The volume of the ionized gas surrounding a hot star, assumed spherical and uniform, is determined by the radius R_s inside which the ionizing photons are absorbed, and therefore is proportional to its ionizing luminosity and inversely proportional to the gas density squared as we showed in the previous section (Eq. 2). The radius of these regions is limited by the rate of ionizing photons (Q_o) emitted by the stars and not by the size of the HI cloud [10]. This cloud remains neutral outside the ionized region. These regions are known as *ionization bounded regions*. However, observations have shown that there exist some regions where there is not enough gas to absorb the ionizing radiation released by the stars. These regions are known as *density bounded regions*.

2.2 Filling factor

The idealization shown above works well as a practical guide to understand the phenomenon in a global way. Nevertheless, the observations show that the structures are more complex than that ideal sphere (see Figure 1). Almost all nebulae show some structure: clumps, filaments, envelopes, density gradients, etc.

Seaton and Osterbrock [13] inferred the existence of strong density fluctuations from the differences in the densities derived from ratios of forbidden lines and from the surface brightnesses measured in $H\beta$.

Osterbrock and Flather [14] studied in detail the density distribution in the Orion Nebula and showed that the densities derived from fluxes at radio wavelengths were considerably less than those derived from the ratio of the forbidden lines [OIII] $\lambda 3729/\lambda 3726$, suggesting that only a fraction of the nebula ($\epsilon \sim 0.03$) is filled with high density fully ionized matter (clumps) and the rest is almost empty. This introduced the “filling factor” concept, defined by

$$\epsilon = \frac{\langle N_e \rangle_{rms}^2}{N_{e,fl}^2} \quad (3)$$

where $N_{e,fl}$ is the electron density determined from the forbidden lines ratio and $\langle N_e \rangle_{rms}$ is the *rms* electron density determined from one Balmer line or from the radio continuum flux.

2.3 Inhomogeneous models

Other models came later [15, 16, 17, 18], some of them really qualitative, but emphasizing the inhomogeneity of the gas and dust distribution in the nebulae. In a semi-quantitative model, Giammanco et al. [17], suggested that the clumps of gas may well be optically thick, so that only a fraction of the clump is ionized. The depth of the ionized portion is then inversely proportional to the square of the distance from the star, so that in all but the nearest clumps only a thin “skin” of any clump is ionized (see Figure 2). A consequence of this model is that considerable neutral gas may exist in an HII region. Another consequence is that the distinction between *ionization bounded regions* and *density bounded regions* is blurred and, generally, a fraction of the ionizing photons could escape, depending on the physical parameters of the region. In this sense every HII region may be density bounded.

Based on this model and defining the *Lyman continuum effective extinction* as $A_{Ly,eff} = -2.5 \log(Q(r)/Q_o)$, where $Q(r)$ is the Lyman continuum luminosity measured at a distance r from the ionizing star, it is possible to show that if the characteristic filling factor of a region is constant, then the ratio $A_{Ly,eff}/A_V$ must be proportional to $1/r$. In the same way, if the filling factor varies, increasing toward the centre as $\epsilon = \left(\frac{\epsilon_o r_o}{r}\right)$, for r much greater than a minimum radius r_o ,

$$\frac{A_{Ly,eff}}{A_V} \sim \frac{1}{\log\left(\frac{r}{r_o}\right)} \quad (4)$$

If the filling factor grows with the radius as $\epsilon = \epsilon_o \left(1 - \frac{r_o}{r}\right)$, for large values of r ,

$$\frac{A_{Ly,eff}}{A_V} \sim \frac{1}{\left(\frac{r}{r_o}\right) - \log\left(\frac{r}{r_o}\right)} \quad (5)$$

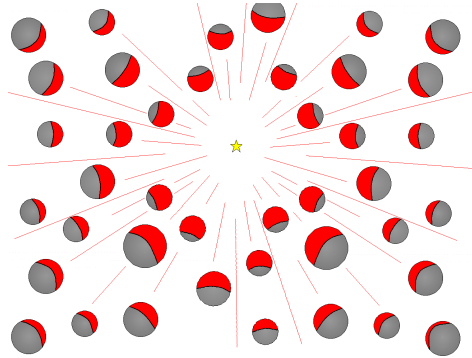


Figure 2: Illustration of the model by Giammanco et al. [17]. The gas is distributed in clumps where only a thin shell is ionized. The thickness of the shell is inversely proportional to the square of the distance to the ionizing star.

3 The data used in this work

M51 (NGC 5194) and its companion NGC 5195 were observed in January 2005 in 4 filters (B , V , I and $H\alpha$) with the ACS (Advanced Camera for Surveys) on board the HST (Hubble Space Telescope). The data were processed with the automatic ACS pipeline [19] and corrected for bias, dark current and flat-field. The different defects of the detector (bad columns, hot pixels, charge transfer efficiency defects, saturated pixels, etc.) were corrected by the Multidrizzle software, a process that also corrects the filter-specific geometric distortion on each image and removes cosmic rays and other undesirable features [20].

From the images acquired with broadband filters we selected all of the sources associated with an HII region. The photometric measurement was done using aperture photometry in the three images B , V , I . With the measured values of luminosity, the absolute magnitudes were then determined, assuming a distance modulus of 29.62 (8.4 Mpc; [21]). Then, colours $B-V$ and $V-I$ were calculated to construct colour-colour diagrams and, from there, we could estimate the V -band extinction for each source. We then assigned to the region the median of the individual V -band extinction, corrected for $H\alpha$ using the extinction curve of Cardelli et al. [22]

In the case of the $H\alpha$ images, we subtracted the continuum emission using a linear combination of the V and I images, properly scaled as described by Knapen et al. [23]. We measured the $H\alpha$ luminosity in ergs s^{-1} , using the conversion factor $\text{PHOTFLAM} = 1.99918 \times 10^{-18} \text{ ergs s}^{-1} \text{ cm}^{-2} \text{ \AA}^{-1}$, the bandwidth of the filter-detector system $\text{PHOTBW} = 37.15 \text{ \AA}$ and the distance to M51 as $2.59 \times 10^{25} \text{ cm}$.

4 Calculation of Lyman continuum and the predicted $H\alpha$ luminosities

Assuming that the absolute magnitude of an O7V star is $V_{O7V} = -4.63$ and that the Lyman continuum luminosity emitted by an O7V star is $Q_{O7V} = 5.62 \times 10^{48}$ photons s^{-1} [12], we computed the total equivalent number of O7V stars (N_{O7V}) in every cluster [24] (i.e. the number of O7V stars that would produce the same luminosity, assuming a Salpeter [25] initial mass function), as well as the Lyman continuum luminosity produced by all of the clusters in a given HII region

$$Q_o = \sum_i N_{O7V}^i \times Q_{O7V}. \quad (6)$$

On the other hand, assuming a dust free ideal region, optically thick to the Lyman continuum radiation [11], the number of ionizing photons to be emitted per second by a stellar population inside a region is given by

$$Q'_o = 2.2 \frac{\lambda_{H\alpha}}{hc} L(H\alpha) \quad (7)$$

where $L(H\alpha)$ is the $H\alpha$ luminosity in ergs s^{-1} and $\lambda_{H\alpha}$ is 6563\AA . This is $Q'_o = 7.27 \times 10^{11} L(H\alpha)$. So, we could compare the two estimated values, Q_o and Q'_o .

5 Results and conclusions

In this work, the analysis is limited to HII regions localized in or around one of the arms of M51, and the minimum distance to the galactic centre is ~ 5 kpc to avoid problems due to overlapping. In general, we did not find any evident correlation between the extinction calculated and the galactocentric distance in the analysed radial interval (see Figure 3). The mean V extinction value of the analysed regions is 1.39 mag, with a minimum 0.4 mag and a maximum 3.6 mag. The Galactic extinction, assumed as $A_{V,G} = 0.116$ mag [26], has been subtracted off to give these values.

Based on the photometric data, we estimated the Lyman continuum emitted by the ionizing sources, assuming an equivalent number of O7V stars and determining the $H\alpha$ luminosity that they should produce in ideal conditions. We compared these values with the extinction corrected $H\alpha$ luminosity measured from the image (see Section 4). The ratio between the *missing* $H\alpha$ luminosity and the *predicted* $H\alpha$ luminosity is on average 0.85.

However, the value of the *Lyman continuum effective extinction*, as defined above $A_{Ly,eff} = 2.5 \log(L_{H\alpha,Ly}/L_{H\alpha})$ [27], where $L_{H\alpha,Ly}$ is the $H\alpha$ luminosity predicted from the broadband clusters luminosity, and $L_{H\alpha}$ extinction corrected measured $H\alpha$ luminosity, is in the range 0.0 – 4.3 mag (with a mean value 1.73 mag), assuming

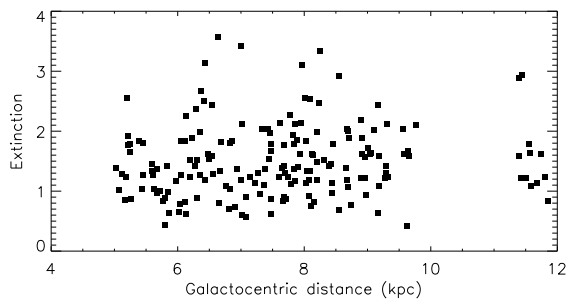


Figure 3: Mean V -band extinction in magnitudes as a function of the galactocentric distance.

that all the missing flux is due to $A_{Ly,eff}$. The mean value of the normalized Lyman continuum effective extinction, $A_{Ly,eff}/E(B - V)$, is 5.5, in the same range as the values of Hill et al. [27]. Plotting this ratio as a function of the region size it is possible to see that the values are limited by an upper envelope (see Figure 4), which shows a slow decline with size.

Some authors have suggested that up to 50 % of the Lyman continuum simply escapes [28, 29], and the lower envelope in the plot in Figure 4 suggests that there may well be a Lyman continuum photon escape factor which increases with the HII region size. Assuming an escape factor as a function increasing with the diameter, with values ranging from 0 to 75%, we applied a correction to the data and derived the plot shown in Figure 5.

This behaviour can be explained only in terms of a highly inhomogeneous gas and dust distribution. Finally, note that the shape of the plot suggests the superposition of a family of functions decreasing with increasing diameter. Could these functions have the shape of the functions presented in section 2.3 for $\frac{A_{Ly,eff}}{A_V}$? If so, these results would strongly support the clumpy model from Giammanco et al. [17]

Acknowledgements:

The work presented here was carried out with the support of projects AYA2004-08251-CO2-01 and AYA2007-67625-CO2-01 of the Spanish Ministry of Education and Science, and P3/86 of the Instituto de Astrofísica de Canarias. LG thanks DGAPA-UNAM, México, for support and the Instituto de Astrofísica de Canarias for hospitality.

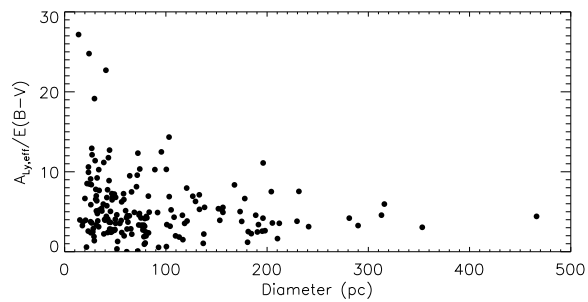


Figure 4: Normalized Lyman continuum effective extinction as a function of the diameter of the region. An upper envelope decreasing with the size and a lower envelope, slowly increasing can be observed.

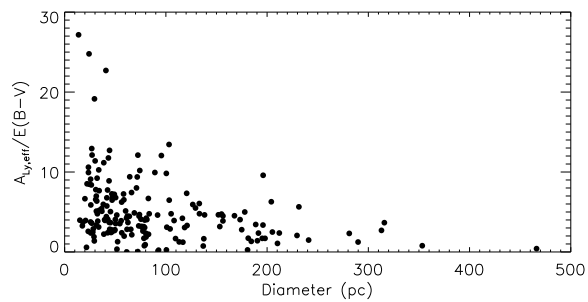


Figure 5: Normalized Lyman continuum effective extinction as a function of the diameter of the region, where the data has been corrected assuming an escape factor increasing with size to a maximum of 75%.

References

- [1] Kennicutt, R.C. 1998, *ARA&A* 36, 189
- [2] Förster Schreiber, N.M., Roussel, H., Sauvage, M., Charmandaris, V. 2004, *A&A* 419, 501
- [3] Chary, R., Elbaz, D. 2001, *ApJ* 556, 562
- [4] Rieke, G.H., Young, E.T., Engelbracht, C.W., et al. 2004, *ApJS* 154, 25
- [5] Calzetti, D., Kennicutt Jr., R.C., Bianchi, L., et al. 2005, *ApJ* 633, 871
- [6] Pérez-González, P.G., Kennicutt, R.C., Gordon, K.D., et al. 2006, *ApJ* 648, 987
- [7] Relaño, M., Lisenfeld, U., Pérez-González, P.G. et al. 2007, *ApJL* 667, 141
- [8] Calzetti, D., Kennicutt, R.C., Engelbracht, C.W., et al. 2007, *ApJ* 666, 870
- [9] Carranza, G., Crillon, R., Monnet, G. 1969, *A&A* 1, 479
- [10] Strömgren, B. 1939, *ApJ* 89, 526
- [11] Osterbrock, D. 1989, in “Astrophysics of Gaseous Nebulae and Active Galactic Nuclei”, Mill Valley: University Science Books
- [12] Martins, F., Schaerer, D., Hillier, D.J. 2005, *A&A* 436, 1049
- [13] Seaton, M.J., Osterbrock, D.E. 1957, *ApJ* 125, 66
- [14] Osterbrock, D., Flather, E. 1959, *ApJ* 129, 260
- [15] Cantó, J., Raga, A., Steffen, W., Shapiro, P.R. 1998, *ApJ* 502, 695
- [16] O’Dell, C.R., Peimbert, M., Peimbert, A. 2003, *AJ* 125, 2590
- [17] Giammanco, C., Beckman, J., Zurita, A., Relaño, M. 2004, *A&A* 424, 877
- [18] Gahm, G.F., Grenman, T., Fredriksson, S., Kristen, H. 2007, *AJ* 133, 1795
- [19] Hack, W.J., Greenfield, P. 2000, “ASP Conf. Ser., Vol. 216, *Astronomical Data Analysis Software and Systems IX*”, eds. N. Manset, C. Veillet, and D. Crabtree (San Francisco: ASP), 433
- [20] Mutchler, M., Beckwith, S.V.W., Bond, H.E., et al. 2005, “Hubble Space Telescope multi-color ACS mosaic of M51, the Whirlpool Galaxy”, *Bulletin of the American Astronomical Society*, Vol. 37, No.2 (<http://www.aas.org/publications/baas/v37n2/aas206/339.htm>)
- [21] Feldmeier, J.J., Ciardullo, R., Jacoby, G.H. 1997, *ApJ* 479, 231
- [22] Cardelli, J.A., Clayton, G.C., Mathis, J.S. 1989, *ApJ* 345, 245
- [23] Knapen, J.H., Stedman, S., Bramich, D.M., Folkes, S.L., Bradley, T.R. 2004, *A&A* 426, 1135
- [24] Vacca, W.D. 1994, *ApJ* 421, 140
- [25] Salpeter, E.E. 1955, *ApJ* 121, 161
- [26] Schlegel, D.J., Finkbeiner, D.P., Davis, M. 1998, *ApJ* 500, 525
- [27] Hill, J.K., Waller, W.H., Cornett, R.H., et al. 1997, *ApJ* 477, 673
- [28] Oey, M.S., Kennicutt, R.C. 1997, *MNRAS* 291, 827
- [29] Relaño, M., Peimbert, M., Beckman, J. 2002, *ApJ* 564, 704

